Chapter 2

Physiological origin of camera-based PPG imaging

Alexei A. Kamshilin[a,b] and Oleg V. Mamontov[b]
[a]*Institute of Automation and Control Processes of Far Eastern Branch of the Russian Academy of Sciences, Vladivostok, Russia,* [b]*Department of Circulation Physiology, Almazov National Medical Research Center, St. Petersburg, Russia*

Contents

2.1 Introduction

The term "photoelectric plethysmography", later transformed to "photoplethysmography" (PPG), was first introduced by Hertzman in 1938 [1]. This technology was proposed to estimate the blood supply of various skin areas. In this pioneering work, the capability of the PPG waveform to follow the time varying changes in blood volume of superficial vessels below the skin during the cardiac cycle was demonstrated. Hertzman called the photoelectrically detectable waveform a pulse volume. Interestingly, over 80 years ago, it was claimed that the amplitude of the pulse volume reflects changes in the blood supply caused by painful and psychic stimuli, cold, amyl nitrite, voluntary apnea, and the Valsalva experiment [1]. Moreover, the parameters affecting the amplitude of PPG waveform were listed and discussed in this pioneering work, among them skin movement relative to the sensing element, variations and spectrum of the illu-

Contactless Vital Signs Monitoring. https://doi.org/10.1016/B978-0-12-822281-2.00010-X

mination, character of the contact of the device with the skin, and the ratio of the reduced to the oxygenated hemoglobin. In 1972, Takuo Aoyaqi proposed to exploit the dependence of the light modulation on the hemoglobin state for noninvasive assessment of arterial-blood-oxygen saturation with an optical device referred to as the pulse oximeter [2,3]. Since 1983, pulse oximeters became commercially available. Today these devices have been adopted to carry out routine measurements in clinics worldwide. The remarkable feature of the PPG waveform to be modulated in time due to the heart contractions is commonly used for estimation and monitoring the heart rate. Currently, PPG modules built into ubiquitous smartphones and watches are used for heart-rate monitoring [4,5]. Moreover, PPG probe serves as a sensitive element in the FINAPRES (an acronym for FINger Arterial PRESsure) system used for continuous measurement of arterial blood pressure [6]. In recent years, there has been increasing interest in expanding the use of PPG beyond these areas. Several studies have been undertaken to prove the ability of the PPG system for assessing pulse-rate variability, pulse-arrival time, vascular tone, tissue perfusion, sympathetic activity, etc. [7–18]. However, despite intensive investigations over a long time and the wide range of applications, the physiological model for the formation of the PPG waveform remains a subject of continuing debate.

In this chapter, we discuss various factors that affect the light modulation of tissue containing vessels with traveling red blood cells (RBC). The most attention will be paid to the reflection mode of the light–tissue interaction, which is typical for a camera-based PPG imaging system. The chapter is organized as following. First, we describe the conventional model of the PPG-waveform appearance, and then the inability of this model to explain the observed largest pulsation amplitude under green illumination is pointed out. Thereafter, an alternative PPG model considering compression of the capillary bed by large arteries is presented and discussed. The rest of the chapter is devoted to a description of experimental observations that support the alternative model.

2.2 Conventional PPG model: blood volume modulation

In any PPG system, a biological tissue is illuminated by an incoherent light source, and the power of light either transmitted through or reflected from the tissue is measured by a photodetector. Correspondingly, there are two modes of operation: transmittance and reflection. In most camera-based PPG experiments, a light source (including ambient illumination) and a light-sensitive camera are located on one side of the biological tissue to be studied, i.e., the PPG imaging system operates in the reflection mode. As is well known, after the light interaction with living tissue containing blood vessels, its intensity acquires modulation in time with the heart rate [19]. The conventional model of the PPG waveform generation was developed on the basis of experimental observations exploiting a pair of light sources and a photodetector in contact with the tissue. It assumes that the main reason for the light-intensity modulation registered by the photodetector is the variation of the blood volume in the tissue [1,12,20–22]. Further in

the Chapter, the conventional model is called a blood-volume (BV) model. This modulation mechanism is easy to understand in the transmittance-mode PPG operating at the near infrared: An increase of blood volume absorbs more photons resulting in a decrease of light intensity measured by the photodetector and vice versa. It is less obvious why the inverse relationship between remitted light power and blood volume should hold in the reflectance-mode PPG, although experimental observations seem to support this standpoint. Therefore, it is generally accepted that PPG measures blood-volume variations in the vascular bed [7,23–26]. The essence of this understanding of PPG signal formation is expressed by the fact that these systems are often called pulse-volume monitor [27–30].

An example of the PPG waveform measured by a camera-based system in the subject's cheek is shown in Fig. 2.1. In this particular example, the subject's face was illuminated by six LEDs arranged around the camera lens, emitting green light at 530 nm with the spectral bandwidth of 40 nm [9]. Raw waveform calculated as a time concatenation of average pixel values in the consecutive frames is shown in Fig. 2.1(A). Averaging was carried out within a selected area sized 7×7 pixels (about 2×2 mm^2). This waveform is presented without any filtering. As can be seen, there are two different terms: an alternating component (AC) with modulation at a frequency of about 1 Hz and a slowly varying component (DC). Both components are proportional to the incident light intensity [31]. By calculating the AC/DC ratio, it is possible to compensate for the spatial unevenness of tissue illumination. In addition, subtracting the unity from this ratio during time-dependence analysis allows one to deal with waveforms with an average level of zero. Usually, AC/DC ratio is measured as a percentage.

For a clearer view of the waveform details, the five-second segment of the PPG waveform in Fig. 2.1(A) is shown in Fig. 2.1(B) after transformations and inversion of the sign. The graph in Fig. 2.1(C) shows a respective segment of the electrocardiogram (ECG) that was recorded simultaneously with video. During recording, the digital camera and ECG were synchronized with an accuracy of one ms. One can clearly see in Fig. 2.1 (B and C) that variations of the light intensity follow the cardiac ejections indicated by R-peaks on the ECG. It should be noted that inverted AC-components correlate positively with variations of arterial blood pressure [32,33]. The relationship of PPG waveform with changes of blood volume was supported by the observed similarity between PPG and simultaneously measured volume of a limb by the strain gauge [34], and by correlation between PPG and arterial diameters measured by Doppler ultrasound [35]. In the systole phase, when the arterial blood pressure reaches its maximum, vessels walls are expanded leading to the maximal momentary blood volume, with reversion to the minimum blood volume as blood runs off in diastole [28]. Therefore, the higher the blood pressure, the greater the blood volume in the arteries, leading to increased light absorption and, accordingly, to a decrease in the pixels value of the camera. Consequently, the minima of the AC/DC ratio shown in Fig. 2.1(C) are reached at the end of diastole when

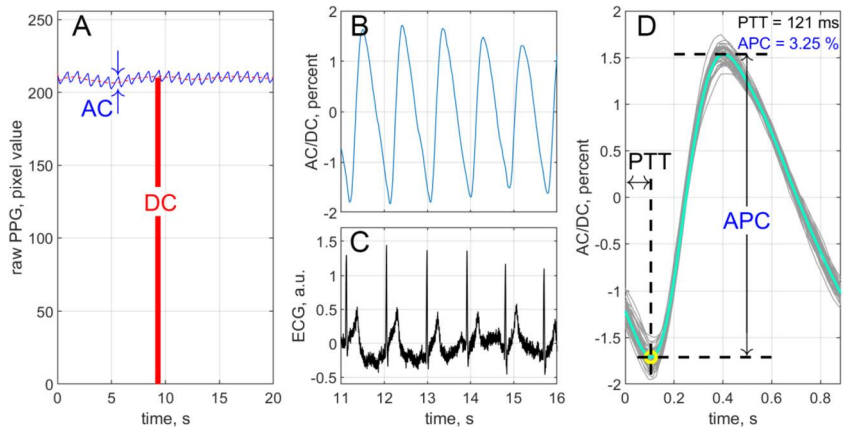

FIGURE 2.1 Typical PPG waveform measured by an imaging PPG system in a subject's cheek under green-light illumination. (A) Raw signal averaged in the region of 7 × 7 pixels (2 × 2 mm^2) without any filtration. (B) The ratio of AC and DC components after low-pass filtering (passband frequency of 20 Hz) and sign inversion. (C) ECG signal synchronously recorded with video frames. (D) One-cardiac-cycle pulse wave (thick green line (mid gray in print version)) obtained after averaging of particular pulse waves (thin gray lines) over 30 cycles.

the blood pressure starts to increase. To verify PPG–ECG correlation, we plotted in Fig. 2.1(D) the PPG pulses of 30 subsequent cardiac cycles, so that each respective R-peak of the ECG is at the beginning of the time scale [9]. The thick greenish line in Fig. 2.1(D) shows an average PPG pulse obtained by averaging the filtered one-cardiac-cycle PPG pulses shown by thin gray lines. The average PPG pulse was used to estimate two important parameters of the PPG waveform. The first is the amplitude of the pulsatile component (APC) which is defined as the difference between maximum and minimum values of the average PPG pulse (Fig. 2.1D). This parameter is usually expressed in percentages. The second is the transit time of the pulse wave from the heart to the measuring point, PTT (pulse transit time), which is the time delay between the R-peak (zero of the abscissa axis in Fig. 2.1D) and the minimum of the average PPG pulse (yellow circle (ligth gray in print version) in Fig. 2.1D). Note that the APC is the amplitude of the AC/DC ratio, which is also referred to as a perfusion index [8,12,36].

2.3 How to explain the largest modulation of the green light?

It should be mentioned that the BV-model, according to which the PPG waveform is treated as originating from pulsatile blood-volume modulation, was developed considering experimental data obtained by contact oximeters operating with red and infrared lights. However, several research groups reported that the largest heartbeat-related AC/DC modulation was observed at the green light [31,37–39]. The conventional BV-model fails to explain these observa-

tions because of the inability of green light to interact directly with pulsatile blood vessels. Usually green light does not penetrate human skin deeper than 0.5 mm [40,41]. There is no pulsating arteries and arterioles at this depth [42], whereas the pulsatile capillary pressure [43,44] and variance in time velocity profile of RBCs [45] are unlikely to exert true blood volume modulation in a single capillary due to the rigid nature of these vessels [46,47].

Nevertheless, many researchers still believe that the conventional BV-model is able to explain features of the PPG waveform with green light, giving the following argument. While the peak of the depth influence of green light is shown to be less than 0.5 mm, some light returning to the surface still can be seen to penetrate deeper into the tissue, most likely encountering subcutaneous arterioles that are probably pulsating. Consequently, this part of the returned light might carry pulsatile (at the heart rate) information. To verify the correctness of this statement, let us estimate the fraction of photons that can reach the arterioles, assuming their location at a depth of 1.2 mm from the stratum corneum. By using statistical analysis of photon diffusion in tissue [48], the probability of the green-light ($\lambda = 560$ nm) fluence at this depth is estimated as $8.25 \times 10^{-4}\%$. This is 3×10^5 times smaller than the fluence probability in the peak depth of 0.5 mm. Most of the light interacts with non-pulsating capillaries, which returns to the detector as the DC component of the PPG. It means that the capillary bed plays the role of efficient screening for light interaction with deeper situated pulsating arterioles. Consequently, the theoretical estimation of AC/DC gives us 0.0032%. In contrast, experimentally measured AC/DC as shown in Fig. 2.1(D) as three orders of value higher (3.25%). This waveform was recorded in the reflection mode by a digital monochrome camera when the subject's face was illuminated by green light (the wavelength of 530 ± 20 nm). RBCs have a peak of light absorption at this wavelength, which leads to the very shallow penetration depth of green light into tissue with blood vessels. Recent rigorous simulation of multiwavelength light–tissue interaction by using a Monte-Carlo model [49] also revealed that green light does not reach the arterioles, interacting exclusively with the upper capillaries.

Therefore, the question arises: Where does the clearly observed modulation at the heartbeat frequency (Fig. 2.1) come from? The same question arises also when analyzing experimental data obtained in PPG systems exploiting a color digital camera. These studies always emphasize that the largest intensity modulation by heartbeats is observed precisely in the green channel of the camera [31,37,39]. It is worth noting that camera-based PPG systems collect light that has traveled through much shallower tissue depths over much smaller distances than takes place in conventional contact PPG probes of oximeters [50,51]. This difference may be due to different net angles of multiple light scattering, which is smaller in the PPG contact sensor, thus forming the characteristic "banana-shaped" optical path. We believe that the heart-related modulation in camera-based PPG systems originates mainly due to mechanical compression/decompression of the intercapillary tissue caused by pulsatile

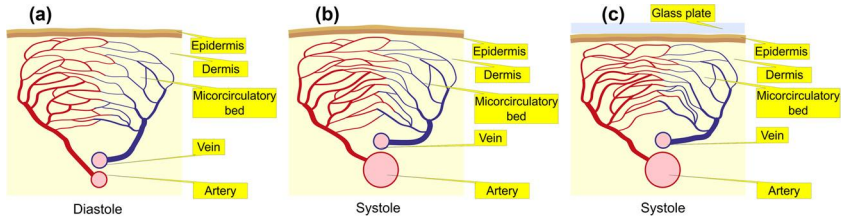

FIGURE 2.2 Simplified diagram of the new concept of the PPG signal formation. (a) A part of the artery that is situated near the dermis in the diastole phase; (b) the artery in the systole phase in the case of free skin surface; (c) the systole phase in the case of skin contact with the glass. Note that the density of vessels in the microcirculatory bed is the lowest in (a) and the highest in (c).

transmural arterial pressure as was suggested by an alternative PPG model in 2015 [33]. Further, this alternative model is called the tissue-compression (TC) model.

2.4 Alternative PPG model: tissue compression modulation

The concept of the TC-model [33] is schematically illustrated in Fig. 2.2. In the end-diastole phase (Fig. 2.2(a)), the arterial pressure is at its minimum, which suggests that tissue located between the artery and epidermis is under minimal compression. In this phase, the reflected light intensity is maximal [37,52], and the inverted AC/DC ratio reaches its minimum, indicated by a yellow circle (light gray in print version) in Fig. 2.1(D). Then the fast increase of the arterial pressure during the systole provides the force affecting the surrounding tissue. The resulting compression of the tissue depends on the boundary conditions, which are defined by the elastic properties of the stratum corneum and epidermis.

Due to the dermis compression, the distance between adjacent capillaries diminishes [53] and leads to an increase of the capillary density that follows the transmural pressure in the location of the measurement. The blood volume interacting with light is certainly larger in more compressed dermis resulting in increased light absorption and a respective growth in the inverted AC/DC ratio after the end-diastole (Fig. 2.1D). It should be noted that mechanical deformations might lead also to changes in the orientation or structure of the connective tissue. Consequently, both the absorption and scattering coefficients of the compressed tissue increase [53], resulting in a decrease in the back-reflected light intensity. However, the relationship between the influence of changes in absorption and scattering coefficients on the formation of the PPG waveform has not yet been established and may vary from one subject to another. The degree of compression depends both on the pressure exerted by the walls of the artery on the adjacent tissue and on the boundary conditions.

2.5 Boundary conditions and influence of skin contact

The effect of the boundary conditions on the degree of dermis compression is illustrated in Fig. 2.2. If the skin motion is not limited by any external contact (Fig. 2.2B), the compression depends primarily on the skin's elasticity. As it was experimentally shown, tighter skin, typical of older people, leads to a greater degree of compression and, accordingly, to a higher APC [54,55]. Note that skin elasticity usually varies spatially across skin areas. In the frames of the TC-model, this variability can explain typically observed heterogeneity of the spatial distribution of APC. Moreover, increased APC is observed in the area of moles or scars, which are also characterized by altered skin elasticity. Dermis compression in the systole phase for the contactless setting is shown in Fig. 2.2(b). One can increase the degree of dermis compression by restricting the skin motion with a glass plate lightly contacting the skin as illustrated in Fig. 2.2(c). A multiple increase in APC (up to seven times) after slight skin contact with the glass plate was experimentally demonstrated by applying imaging PPG with green light to assess blood pulsations in subjects' palms [33,56]. Such a large enhancement of the heart-related modulation amplitude cannot be explained in the framework of the conventional BV-model. Note that the external pressure caused by the glass-plate contact in these experiments was on average of 35-mm Hg [55], thus preventing occlusion of the blood vessels. The frequently observed improvement of the waveform shape by an external force in contact PPG probes [25,57,58] can be also associated with changes in mechanical properties of the tissue. Noise-like PPG waveforms observed without skin-probe contact might be caused by inefficient transmission of the pressure wave from the arteries to the capillary bed, whereas the contact restricts skin motion and provides conditions under which pulsatile arterial pressure efficiently modulates the capillary density.

2.6 Pulsatile dermis compression and modulation of IR light

Even though the reflection-mode oximeters operate at the frequencies of red and near-infrared light, which penetrates much deeper than green light, the influence of the dermis compression should be also significant for the infra-red light because any light interacts twice with upper level of the dermis before reaching the photo-receiver. Such an influence was observed in the experiments with simultaneous measurements of PPG signals at green (525 nm) and NIR (810 nm) illuminations in the palms of 34 healthy subjects [56]. In these experiments, the temporal modulation of both wavelengths was assessed in a quasi-synchronous mode. A single monochrome camera was used to record images of the subjects' palms when they were illuminated with rapidly switching green and NIR light emitted by different LEDs synchronized with the camera. A trigger pulse generated by the camera at the beginning of each frame switched on either green or NIR LEDs. Thus, each even-numbered camera frame was recorded when the palm was illuminated by green LEDs, but each odd-numbered frame by NIR

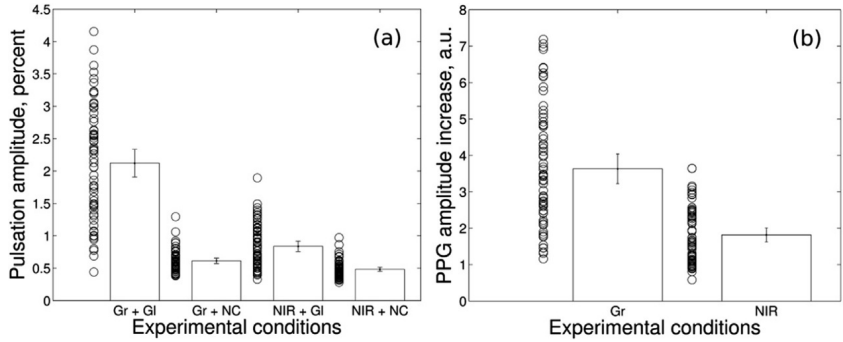

FIGURE 2.3 Influence of the skin-glass contact on the PPG amplitude measured at green and NIR wavelengths. (a) Average PPG amplitude measured in the contact experiment (Gl) and in the same areas in the contactless experiment (NC). Here Gr and NIR stand for green (525 nm) and NIR (810 nm) illumination, respectively. (b) Ratio of the mean amplitude measured in the glass-contact to that in the contactless experiment for both wavelengths. The individual measurements are shown by circles, whereas the bars represent mean values for the whole data sets.

LEDs [56]. A strong positive correlation between the changes caused by the skin contact with a glass plate in both wavelengths was found, suggesting that the same signal was read independently from the depth of penetration. Specifically, changes in APC due to the skin contact were found to be correlated for the two wavelengths both in space and in amplitude. The glass plate increased APC measured at NIR illumination at the same locations as with green-light illumination [56]. It was also found that the contact with glass increased the light modulation up to seven times with green illumination and up to 3.6 times with NIR illumination (see Fig. 2.3b).

Analysis of the data shows that an essential part of remitted NIR light is modulated in time as a result of elastic deformations of dermis caused by variable blood pressure in the arteries [56]. These observations suggest that, in contrast with the classical BV-model, photoplethysmographic waveform originates from the density modulation of the upper capillaries due to the variable pressure applied to the dermis from large blood vessels. Given that camera-based PPG imaging is at the heart of the development of contactless methods for measuring oxygen saturation [50,59], application of the TC model in the development of algorithms for new SpO_2 measurement systems can improve the accuracy of their calibration.

2.7 Light modulation in a single capillary

The alternative TC-model is based on the assumption that blood volume modulation in a single capillary at a heart rate is unlikely. Let us take a closer look at this issue. On the one hand, the average density of capillaries in human tissue is approximately 600/mm^3, which implies a mean separation of about 40 μm between adjacent capillaries, with their average length 1.1 mm and their average

diameter about 8 μm [60]. On the other hand, the average size of human RBCs is of the same order of value [61]. In these conditions, one hardly can assume that the amplitude of blood volume pulsations in the same vessels might grow up to seven times after slight contact with glass. Nevertheless, such a large increase in the pulsation amplitude when the skin motion is restricted by light contact with a glass plate (see Fig. 2.3b) was experimentally demonstrated [56].

Detailed study of the PPG signal formation in the spatially resolved images of nailfold capillaries provided by a microscope [45] revealed that the spatial distribution of APC does not always coincide with the position of visible capillaries (see Fig. 2.4). Note that, unlike the experiments discussed in the previous sections that used a monochrome camera and active illumination by green light, this study used a color camera and white light. However, only the green channel of the color camera was processed as having the highest SNR [45]. As seen in the lower part of Fig. 2.4(b) (in the region with higher density of capillaries), the amplitude of pulsations is higher than in the upper part with a single layer of capillaries, and it has almost uniform distribution. Despite the significant amplitude of heart-related pulsations of the reflected green light, no modulation of the capillaries' diameter in the time course was observed in magnified capillary images [45]. However, it should be noted that the RBC speed in each capillary was found to be strongly modulated following the heartbeats. Nevertheless, the modulation of RBC speed cannot directly lead to the light-intensity modulation due to the relatively high speed of RBCs and the strong difference of the average speed (more than ten times) between adjacent capillaries. It should be noted that the observed speed of erythrocytes in capillaries is so high that it leads to their significant displacement in capillaries during the timescale of heartbeats. Typical frame-exposure time accepted for the signal acquisition in imaging PPG systems is about 25 ms. During this period, the number of erythrocytes in a region of interest is independent of their speed, if we assume their density is almost constant.

Under this assumption, the number of photons absorbed by moving erythrocytes is proportional to the exposure time and mean cross-section of RBCs. Therefore, modulation of RBC speed cannot directly lead to the light intensity modulation [45]. In addition, significant diversity of the RBC speed observed in various different capillaries cannot lead to the in-phase modulation of the remitted light intensity in the whole area of observation.

While the conventional BV-model fails to explain the features of RBC dynamics observed under a microscope, the alternative TC-model [33] does this successfully. It is worth noting that Volkov et al. [45] also suggested the presence of one more mechanism capable of modulating the absorption of light by RBCs due to their speed modulation in nonpulsatile capillaries. It is based on the experimental evidence of the light-absorption dependence on the RBCs orientation and aggregation that varies with their speed [62,63]. With an increase in RBCs speed, a decrease in light absorption and scattering is usually observed [63]. However, such a dependence means that the light intensity measured in the

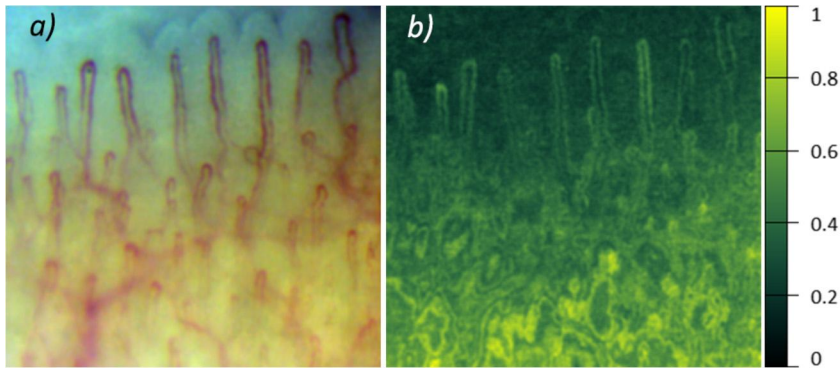

FIGURE 2.4 Mapping the amplitude of PPG waveform. (a) Microscopic image of capillaries. (b) Spatial distribution of the PPG-signal amplitude calculated for the green channel of the image. The color scale on the right side shows the amplitude of the normalized PPG signal (maximum value is 1).

systole (when the RBC speed is higher) will be higher than in the diastole. In other words, this modulation is in counter phase to that predicted by either BV or TC model. Therefore, the mechanism of light modulation due to changes in the RBCs shape/orientation could just diminish experimentally observed APC.

2.8 Irregularity of RBC motion

The predictive ability of the TC-model was demonstrated recently in a new method for capillary visualization in any part of the body [64]. This method is based on the difference of PPG waveforms recorded under a microscope in areas with and without visible skin capillaries containing moving RBCs. It was shown [64] that the modulation of light in the regions between the capillaries has a much more regular shape than in the capillary itself. Fig. 2.5 shows PPG waveforms and their spectra recorded in four regions of interest (ROI) with a size of 4.1 $\times$ 4.1 μm^2. The color of the curves in Fig. 2.5 identifies the ROI position: Red (mid gray in print version) and pink (light gray in print version) were located inside the capillary with moving RBCs, whereas blue (dark gray in print version) and green (gray in print version) were outside the capillaries.

As seen in Fig. 2.5, PPG waveforms outside capillaries (blue and green curves) have regular modulation at the heartbeats, whereas the light intensity modulation is much more random in ROIs selected within capillaries (red and pink curves). We explain this difference as follows. Random, noise-like modulation originates from the inhomogeneity of RBC density in capillaries and their motion. Some of the RBCs are joined together forming aggregates of various lengths [65]. Motion of these aggregates separated by plasma produces noise-like light flickering. Since RBC-plasma sequences and their speeds are different in different capillaries, multiple light interaction with various capillaries smooths over the flickering and leads to more regular modulation of the heart

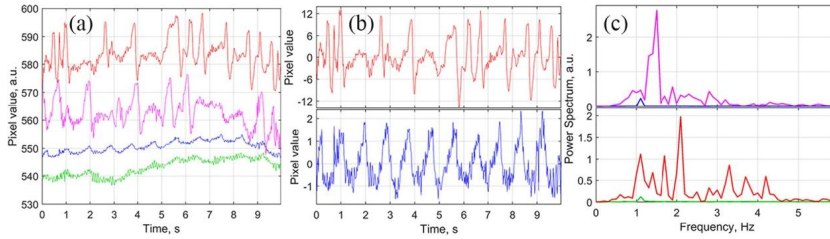

FIGURE 2.5 Particular realizations of PPG waveforms and their spectra. (a) Evolution of the mean pixel value (without any filtration) estimated in four selected ROIs: red (mid gray in print version) and pink (light gray in print version) are inside the capillaries with moving RBCs, whereas blue (dark gray in print version) and green(gray in print version) are outside. (b) PPG waveforms after removal of slowly varying changes in the red and blue ROIs. (c) Power spectra of PPG waveforms in all the selected ROIs.

rate. We suggest that the origin of the heart-related light modulation outside the capillaries is the compression/decompression of the dermis by the pulsatile arteries. Therefore, the superficial capillary layer can be considered as a distributed sensor for monitoring the parameters of blood pulsations occurring in the arteries.

2.9 Occlusion plethysmography

The TC-model served also as a starting point for the development of new applications of the PPG system as a monitor for peripheral blood flow changes during venous occlusion. In this physiological maneuver, return of venous blood is briefly interrupted for four–ten s by inflating a brachial cuff still allowing arterial blood flow into the limb. The rate of blood flow is assessed by estimating the changes in the limb's volume caused by the incoming blood. Usually it is done with either a strain gauge (which measures variations of limb's circumference) [66] or air plethysmography (which measures pressure changes in an air chamber contacting the limb) [67]. There is contact between the skin and sensor in both plethysmography techniques. Evidently, the arterial blood inflow during venous occlusion leads to the increase of the limb's volume and may compress the tissue between the skin and veins. Taking into account the TC-model, we hypothesized that such compression can lead to an increase in the green-light absorption in the capillary layer and therefore to a decrease in the signal measured by an imaging PPG system. This hypothesis was experimentally confirmed [68], resulting in a proposal for a contactless method for the assessment of blood flow reactivity in the limbs [69]. In fact, during the venous occlusion, the blood is accumulating in venules and veins, which is observed by an imaging PPG system as a linear decrease in the DC component.

The typical evolution of the PPG signal during multiple venous occlusions is shown in Fig. 2.6. Note that it was obtained under green illumination of the forearm [69]. Green arrows (dark gray in print version)indicate the beginning of

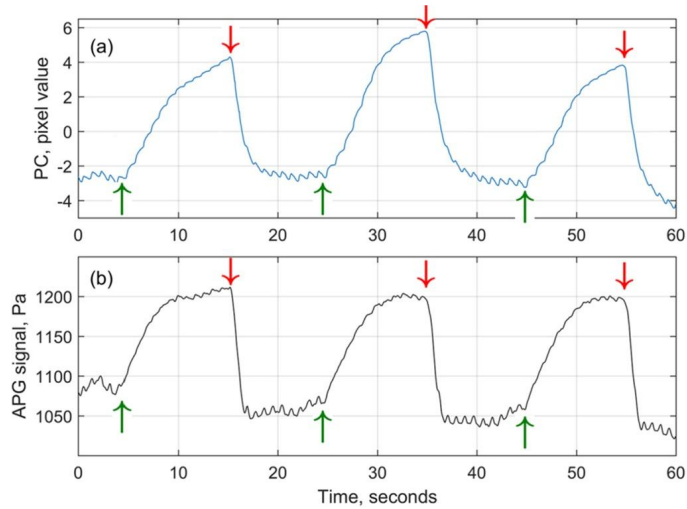

FIGURE 2.6 Comparison of imaging-PPG and air-plethysmography (APG) waveforms in response to triple venous occlusion. (a) PPG waveform, (b) APG waveform. While green arrows (dark gray in print version) show the beginning of each occlusion, the red arrows (gray in print version) indicate the moments of occlusion cuff deflation.

each venous occlusion, whereas the red arrows (gray in print version) show the end of each occlusion. Similarly to the conventional processing of PPG waveforms (see Sect. 2.2), here we subtracted the average value of the signal and changed the sign. One can clearly see in Fig. 2.6(a) that the PPG signal linearly increases immediately after the beginning of the cuff inflation and sharply returns to the initial level after the cuff deflation. This waveform is very similar to the simultaneously recorded, gold standard air-plethysmography (APG) signal shown in Fig. 2.6(b): The beginning and end of each occlusion event are well-synchronized. Moreover, small oscillations at the frequency of about 1 Hz attributed to arterial blood pulsations at the heart rate are in phase in both waveforms. It was found that the heart-related pulsations are resolved even in the occlusion state, but their amplitude (APC) is smaller than before occlusion [69]. The observed diminishment of the heart-related pulsations in the course of occlusion (Fig. 2.6) can be explained by the decrease in the pressure difference applied to a capillary due to the increased pressure in the venules.

Again in this experiment, the venous occlusion was monitored using green light that penetrates only into the superficial layer of the dermis. Therefore, the reason for the observed light-absorption increase is the increase of the blood volume in the superficial layer. This increase can be explained in the framework of the TC-model. Blood accumulating in the veins increases the pressure on the upper layer of the capillaries and squeezes this layer, reducing the distance between the capillaries. Once again, the capillary bed serves as a distributed sensitive network for monitoring the state of deep blood vessels, both arteries

and veins. The change in green-light absorption during occlusion can be also explained by an increase in blood volume in small venules that are situated closer to the superficial layer of capillaries than arterioles. Currently, the details of the mechanism for the light modulation in the capillary bed is still under debate. Additional theoretical and experimental studies are required to determine the relationship between the two mechanisms (BV and TC) of green-light modulation by the blood-filling veins during venous occlusion. Nevertheless, recent mathematical simulations of light penetration into the dermis by using the Monte-Carlo method [49,70] demonstrated the low probability that green light interacts with venules or arterioles, thus supporting the predominant role of the TC-model in the formation of a response to venous occlusion. In any case, both mechanisms are able to explain the experimentally observed independence of the PPG-signal-changes rate from the observation point. It was shown that the response of the green-light PPG system to venous occlusion does not depend on the positioning of the observation point along the limb (upper or lower), or surrounding it [69,71].

2.10 Peculiarities of light interaction with cerebral vessels

The previous sections discussed the formation of a PPG waveform during the light interaction with skin capillaries, whereas in this section the PPG signal originating from vessels of the cerebral cortex is considered. Unlike the network of vessels supplying the dermis with blood, the vascular bed of cerebral vessels is arranged differently. As known, the main blood supply to the brain is carried out by meningeal vessels penetrating the brain tissue from the side of the convexital surface [72]. These vessels depart from the Willis circle as paired anterior, middle, and posterior cerebral arteries and further ramify on gyri of the cerebrum, gradually decreasing in diameter from 700 to 40 μm from the conducting to the precortical arteries. Next, from each precortical artery, two–three cortical arteries depart, which penetrate into the cortical space at right angles [72]. Therefore, pulsatile arteries of medium and small caliber are located on the surface of the cerebral cortex and can directly interact with green light. Accordingly, oscillations of the blood volume in the arteries primarily lead to the modulation of green light with the heart rate. This fact was confirmed in the experiments with rats carried out in our group [73]. Fig. 2.7 shows mapping of APC in the open brain cortex.

From the network of blood vessels resolved in the instant, unprocessed frame shown in Fig. 2.7(a), it is difficult to determine which are the arteries and which are the veins. Nevertheless, mapping of the pulsation-amplitude parameter, APC, visualizes exclusively arteries, which is clearly seen in Fig. 2.7(b) where the arteries are highlighted by red (dark gray in print version) as having much higher amplitudes of pulsations. Since in this case green light initially interacts with pulsatile vessels, its heart-related modulation can be explained in frames of the BV-model. However, we cannot completely exclude the presence

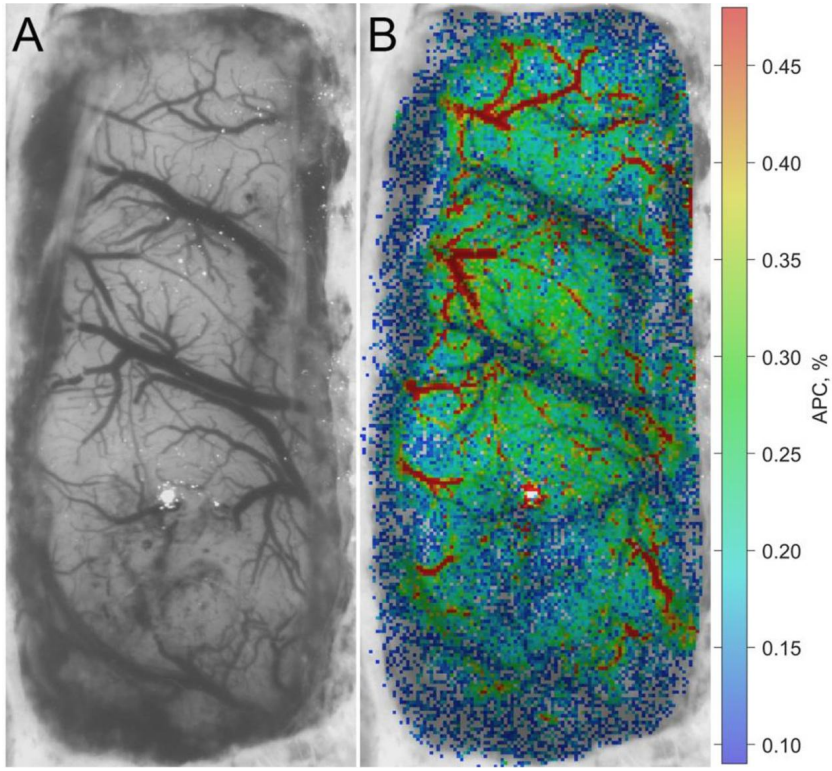

FIGURE 2.7 Spatial distribution of APC in brain cortex. (A) One of the recorded video frames of the open rat's brain, and (B) spatial distribution of APC overlaid with the initial image. The color scale on the right shows AC/DC ratio in percent.

of light modulation due to periodical compression of the brain tissue by large pulsating arteries (TC-model), some of them situated below the visible cortex. The influence of the TC-model becomes more pronounced in an exemplary APC map (see Fig. 2.8) obtained in the human cortex that was opened up during neurosurgical intervention [74].

As can be seen, regions with higher APC (highlighted by red-yellow (dark gray-light gray in print version) in Fig. 2.8B) do not necessarily coincide with the structure of the arteries visible in Fig. 2.8(A). Moreover, the APC is almost uniformly distributed within areas bounded by blue-highlighted, non-pulsating veins in the left part of Fig. 2.8(B), whereas such distribution is more uneven in the upper-right part. Despite the fact that veins, the area of which is approximately double that of the area of arteries, occupy a significant part of the cerebral cortex, these vessels do not contribute in APC. The obvious explanation for this is the significantly lower blood-flow velocity through the veins, the pulsation of which is at least an order of magnitude lower than in the arteries. It is worth

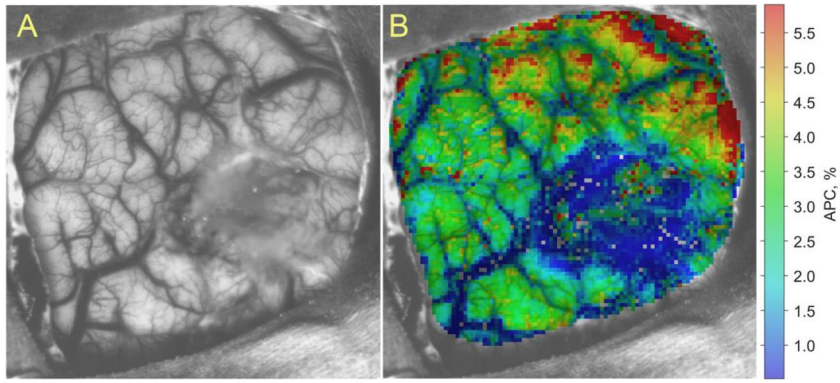

FIGURE 2.8 Mapping the blood pulsations parameters in a brain cortex. (A) One of the recorded video frames of the subject's brain opened up during neurosurgery, and (B) spatial distribution of APC overlaid with initial image. The color scale on the right shows AC/DC ratios in percent.

noting that the mean APC in human cortex (Fig. 2.8 b) is ten times higher than in the rat's cortex (Fig. 2.7B).

2.11 APC as a measure of the arterial tone

Regardless of whether the change in blood volume happens in the pulsating arteries or in the capillary bed when it is compressed by the arteries causes light modulation, the main reason for the modulation is pulse pressure, i.e., the pressure difference in systole and diastole at the point of measurements. However, there are other mechanisms that can affect the amplitude of changes in the lumen of the arteries at the same pulse pressure. For example, the products of brain tissue metabolism, of which CO_2 is of the greatest importance, most actively control the lumen of meningial vessels [75,76]. Despite the fact that large cerebral vessels are involved in autoregulation of cerebral blood flow, the leading role belongs to the meningeal arteries, which determine about 40% of vascular resistance and incorporate specialized sphincters affecting the volumetric flow rate [72]. The tone of the sphincters is determined by metabolic factors and, exerting a regulatory effect, brings into correspondence the trophic need of the brain for blood supply. A decrease in sphincter tone leads to a decrease in local vascular resistance and a corresponding increase in pulse pressure [77]. This increase leads to an increase in the amplitude of arterial lumen oscillations. These oscillations in the lumen determine the variable-in-time component of the PPG waveform. When light interacts directly with arteries, changes in the lumen modulate the absorption of light. In the case of interaction mainly with nonpulsating capillaries, pressure fluctuations change the compression of the tissue, thereby modulating the absorption of light again.

The effect of arterial tone on APC measured in green-light imaging PPG system has been demonstrated in recent experiments to study rats' cerebrovas-

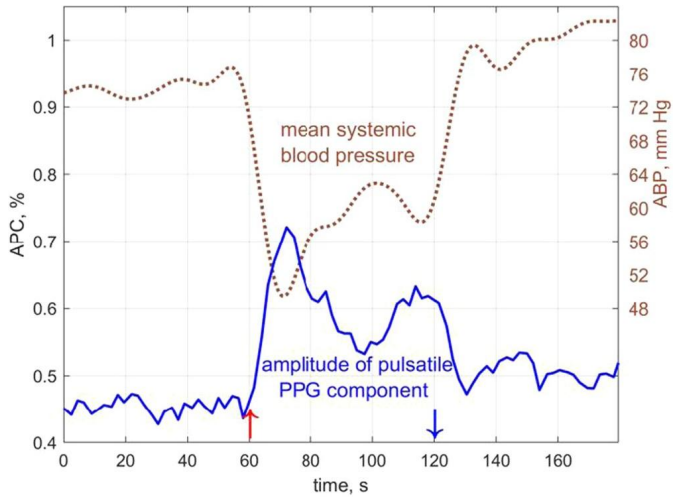

FIGURE 2.9 Typical dynamics of the mean systemic blood pressure (dashed brown curve) and APC (solid blue curve) in cerebral arteries of a rat during painful visceral stimulation. Red (darkgray in print version) and blue (gray in print version) arrows near the X-axes show the beginning and end of the stimulation, respectively.

cular responses to pain stimuli [73]. Simultaneous recording of the systemic blood pressure and imaging PPG in the open rat's brain revealed counter-phase changes in the blood pressure and APC as shown in Fig. 2.9. One can see that painful visceral stimuli (applied at 60 s in the trial) leads to a decrease in systemic arterial pressure accompanied by an increase in APC, whereas the pressure increase at the end of stimuli results in a decrease in APC.

These observations can be explained by a reflex change in the tone of cerebral vessels in response to changes in perfusion pressure [73]. This reaction is in line with the features of the cerebrovascular reflex, the physiological role of which is to maintain the constancy of cerebral blood flow regardless of fluctuations in the systemic blood pressure [78]. In other words, APC follows the local vascular resistance that is varying under the influence of systemic arterial pressure. Therefore, the parameter APC of PPG waveform can be considered as a measure of the cerebral vascular tone.

2.12 Green-light camera-based PPG and cutaneous perfusion

As just discussed, when an imaging PPG system is utilized to measure vascular parameters through the skin, green light interacts predominantly with the superficial layer of capillaries. Given the noncompliance of capillaries with minor change of their size due to blood pressure change (the blood volume in the capillaries does not pulsate) [46], one may ask: Is camera-based PPG suitable for measuring cutaneous blood perfusion? This question received a positive

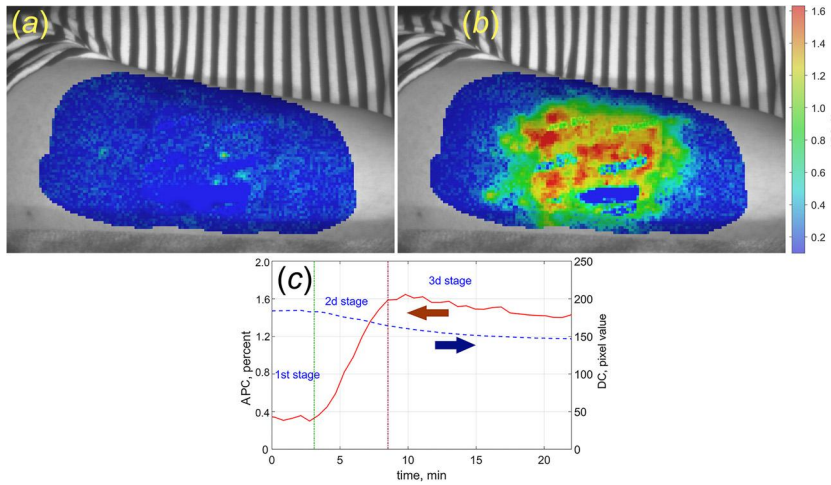

FIGURE 2.10 APC mapping in the area of the capsicum-patch application to the upper arm in the second (a) and twelfth minute (b) after the patch application. The color scale on the right of the maps shows APCs in percent. Evolution of APC averaged within the patch area is shown in the graph (c) by the solid red line, whereas the dashed blue line shows evolution of the mean DC component of the PPG waveform.

answer in experiments on monitoring the effect of capsaicin-patch application on microcirculation [18]. In this experiment, a capsicum patch was attached to a subject's upper arm and illuminated by green light, while video of the forearm was continuously recorded. Video and ECG recording started two minutes prior to the plaster application. The transparency of the capsaicin patch to green light allowed measuring the spatial distribution of APC and its dynamics continuously during the whole period of patch application. APC mapping at the second and twelfth minute after application of the patch are shown in Fig. 2.10(a) and 2.10(b), respectively. In both examples, the APC maps were drawn in pseudo-colors using the same color scale shown on the right side of the images. A fourfold increase in pulsation amplitude after twelve minutes is clearly visible.

The solid red line in Fig. 2.10(c) shows representative examples of the evolution of the APC averaged over the patch area. At the beginning of the patch application, the small APC was observed for all 28 subjects under study [18]. After a certain delay time, APC began to grow rapidly. The delay time varied for each subject, with the mean value of 7.6 ± 3.5 m ranging from 1.1 to 13.9 m. In all cases, the time-course of APC changes after capsaicin application consisted of three clearly distinguishable stages. The first stage was represented by a latent period when the heartbeat related modulation was of rather small amplitude. At the second stage, a sharp increase of APC was observed, and then, in the third stage, APC was saturated.

A typical reaction of the application of capsaicin to human skin is progressive redness of the skin [79], which becomes apparent as an increase of green-light absorption. Therefore, the skin redness (or hyperemia) could be estimated as the relative change of the DC component of the PPG waveform measured in the location of the patch. The evolution of the DC component is shown in Fig. 2.10(c) by a dashed blue line. As seen, variations of the DC component is significantly smaller than that of APC. In the group of 28 subjects, the relative change in the DC component during the second stage of the patch application is much smaller than in the AC component ($8.3 \pm 4.2\%$ versus $220 \pm 100\%$) [18].

Capsaicin is known to release the calcitonin gene-related peptide (CGRP), which leads to a potent dilatation of cutaneous arteries [80,81]. However, observed capsaicin-induced hyperemia as the change in DC component suggests variations of the RBCs number in the superficial capillary layers to be less than 10% ($8.3 \pm 4.2\%$). Under these conditions, the concomitant four-fold increase in APC (Fig. 2.10(c)) can hardly be explained within the framework of the conventional BV-model. In contrast, the TC-model explains the functional test with capsaicin as follows. As in cerebral vessels, a decrease in sphincter tone (due to release of CGRP) results in an increase in the pulse pressure with a corresponding increase in the amplitude of the arterial lumen oscillation. Therefore, the increased pulsation amplitude of the arteries more strongly compresses the upper capillary layer, thus increasing the AC component of the PPG waveform. At the same time, the decreased arterial tone results in a decrease in local vascular resistance [77] and respective increase of RBC velocity, which causes the increase of cutaneous blood perfusion. Note that the increasing perfusion occurs mainly due to higher RBC speed under conditions of a slightly changing total number of RBC. In other words, capsaicin increases the number of functioning capillaries: Before capsaicin is applied, RBCs fill non-functional capillaries, but their velocity is close to zero, whereas, after the decrease in arterial tone, RBCs begin to move in the capillaries. This is in line with video-capillaroscopy observations showing that the higher mean RBC velocity is associated with higher amplitude of velocity modulation of an almost constant number of RBCs [45]. Therefore, the APC parameter of imaging PPG allows assessment of the cutaneous perfusion and its response to various functional stimuli.

Assessment of the microcirculation response on the local thermal impact using the camera-based PPG system [82] demonstrated also that the temperature-induced increase in the normalized pulsation amplitude is mainly driven by the growth of the pulsatile AC component of the PPG waveform. In this experiment, six–eight independent trials of internal warming of the previously cooled finger were carried out for each of nine subjects. It was found that within ten s of a local increase in the temperature of the finger's skin, the AC component increased by 7.1 ± 2.5 times, whereas the DC component dropped by only $17 \pm 6\%$ [82]. This experiment also underlines the importance of the TC-model of PPG signal formation for implementation of the experimental observations. Moreover, recent experiments on local external heating of the forehead demonstrated the

applicability of the camera-based PPG method to measure quantitatively the vasomotor response to local thermal exposure [10]. It was found that APC is a very sensitive marker of changes in skin blood flow that are observed in response to local heating of the forehead skin. Local heating of about 5 °C results in a several-fold APC increase, which is well localized in the heating area. In most cases, the increase in BPA continues after the cessation of heat exposure and the respective diminishment of the skin temperature. Likewise, in the experiment with capsaicin patch application, the increase in cutaneous perfusion is also associated with activation of temperature-sensitive vanilloid receptors of the temporary potential (TRPV) via CGRP. Once again, this activation leads to a decrease in arterial tone, an increase in their pulsation amplitude, and a respective increase in the amplitude of the superficial capillary-layer compression that results in an increase in APC.

2.13 Conclusive remarks

In this chapter, we have discussed the relationship between the two main physiological models (blood-volume, BV, and tissue-compression, TC) for the interaction of light with biological tissue containing *in-vivo* blood vessels. In fact, both models agree that the reason for the modulation of light is the modulation of its absorption due to changes in the volume of blood with which it interacts. The difference is where exactly and for what reasons these changes in blood volume occur. If the conventional BV-model does not specify the source of blood pulsations, proposing that it is most likely arteries and arterioles, then the TC-model pays special attention to the change in blood volume in the superficial capillary layer. We have cited a number of recent experimental studies, the results of which support the TC model and clearly show the need to take into account the mechanical properties of the capillary bed.

One of the conclusions of our analysis is that the superficial capillary layer serves as the distributed network allowing quantitative characterization of the mechanisms of systemic vascular regulation. Moreover, the analysis of light modulation caused by interaction with tissue containing blood vessels makes it possible to reliably identify and objectively assess disorders of local microcirculation and systemic hemodynamics, thereby assessing neurogenic vasomotor reactivity, which is very important for maintaining systemic hemodynamic parameters. Deeper study the basic aspects of light interaction with living tissue is extremely important for both correct interpretation of the experimental data and development of new noninvasive, contactless diagnostic instrument. Further progress in clarifying the physiological mechanism behind PPG will make possible the development of new methods for the early diagnosis of socially significant diseases such as complications of diabetes mellitus; obliterating vascular diseases of the lower limbs; systemic sclerosis; skin, stomach, and intestines cancer; and others.

Acknowledgments

This study was funded by the grant from the Ministry of Science and Higher Education of the Russian Federation (agreement 075-15-2020-800).

References

[1] A.B. Hertzman, The blood supply of various skin areas as estimated by the photoelectric plethysmograph, Am. J. Physiol. 124 (1938) 328–340, https://doi.org/10.1152/ajplegacy.1938.124.2.328.

[2] T. Aoyagi, M. Kishi, K. Yamaguchi, S. Watanabe, Improvement of earpiece oximeter, Osaka (1974) 90–91.

[3] J.W. Severinghaus, Y. Honda, History of blood gas analysis. VII. Pulse oximetry, J. Clin. Monit. Comput. 3 (1987) 135–138, https://doi.org/10.1007/BF00858362.

[4] R-C. Peng, X-L. Zhou, W-H. Lin, Y-T. Zhang, Extraction of heart rate variability from smartphone photoplethysmograms, Comput. Math. Methods Med. 2015 (2015) 516826, https://doi.org/10.1155/2015/516826.

[5] B. Sanudo, M. De Hoyo, A. Munoz-Lopez, et al., Pilot study assessing the influence of skin type on the heart rate measurements obtained by photoplethysmography with the apple watch, J. Med. Syst. 43 (2019) 195, https://doi.org/10.1007/s10916-019-1325-2.

[6] B.P.M. Imholz, W. Wieling, G.A. van Montfrans, K.H. Wesseling, Fifteen years experience with finger arterial pressure monitoring: assessment of the technology, Cardiovasc. Res. 38 (1998) 605–616, https://doi.org/10.1016/S0008-6363(98)00067-4.

[7] M. Nitzan, A. Babchenko, B. Khanokh, D. Landau, The variability of the photoplethysmographic signal – a potential method for the evaluation of the autonomic nervous system, Physiol. Meas. 19 (1998) 93–102, https://doi.org/10.1088/0967-3334/19/1/008.

[8] A.P. Lima, P. Beelen, J. Bakker, Use of a peripheral perfusion index derived from the pulse oximetry signal as a noninvasive indicator of perfusion, Crit. Care Med. 30 (2002) 1210–1213, https://doi.org/10.1097/00003246-200206000-00006.

[9] A.A. Kamshilin, T.V. Krasnikova, M.A. Volynsky, et al., Alterations of blood pulsations parameters in carotid basin due to body position change, Sci. Rep. 8 (2018) 13663, https://doi.org/10.1038/s41598-018-32036-7.

[10] M.A. Volynsky, N.B. Margaryants, O.V. Mamontov, A.A. Kamshilin, Contactless monitoring of microcirculation reaction on local temperature changes, Appl. Sci. 9 (2019) 4947, https://doi.org/10.3390/app9224947.

[11] B. Khanokh, Y. Slovik, D. Landau, M. Nitzan, Sympathetically induced spontaneous fluctuations of the photoplethysmographic signal, Med. Biol. Eng. Comput. 42 (2004) 80–85, https://doi.org/10.1007/BF02351014.

[12] A. Reisner, P.A. Shaltis, D. McCombie, H.H. Asada, Utility of the photoplethysmogram in circulatory monitoring, Anesthesiology 108 (2008) 950–958, https://doi.org/10.1097/ALN.0b013e31816c89e1.

[13] J. Lee, K. Matsumura, T. Yamakoshi, et al., Validation of normalized pulse volume in the outer ear as a simple measure of sympathetic activity using warm and cold pressor tests: towards applications in ambulatory monitoring, Physiol. Meas. 34 (2013) 359–375, https://doi.org/10.1088/0967-3334/34/3/359.

[14] N. Blanik, A.K. Abbas, B. Venema, et al., Hybrid optical imaging technology for long-term remote monitoring of skin perfusion and temperature behavior, J. Biomed. Opt. 19 (2014) 16012, https://doi.org/10.1117/1.JBO.19.1.016012.

[15] T.Y. Abay, P.A. Kyriacou, Reflectance photoplethysmography as noninvasive monitoring of tissue blood perfusion, IEEE Trans. Biomed. Eng. 62 (2015) 2187–2195, https://doi.org/10.1109/TBME.2015.2417863.

[16] A.A. Kamshilin, I.S. Sidorov, L. Babayan, et al., Accurate measurement of the pulse wave delay with imaging photoplethysmography, Biomed. Opt. Express 7 (2016) 5138–5147, https://doi.org/10.1364/BOE.7.005138.

[17] K. Matsumura, K. Shimuzu, P. Rolfe, et al., Inter-method reliability of pulse volume related measures derived using finger-photoplethysmography, J. Psychophysiol. 32 (2018) 182–190, https://doi.org/10.1027/0269-8803/a000197.
[18] A.A. Kamshilin, M.A. Volynsky, O. Khayrutdinova, et al., Novel capsaicin-induced parameters of microcirculation in migraine patients revealed by imaging photoplethysmography, J. Headache Pain 19 (43) (2018), https://doi.org/10.1186/s10194-018-0872-0.
[19] A.B. Hertzman, C.R. Spealman, Observations on the finger volume pulse recorded photoelectrically, Am. J. Physiol. 119 (1937) 334–335, https://doi.org/10.1152/ajplegacy.1937.119.2.257.
[20] J. Nieveen, L.B. van der Slikke, W.J. Reichert, Photoelectric plethysmography using reflected light, Cardiologia 29 (1956) 160–173, https://doi.org/10.1159/000165601.
[21] J. Weinman, A. Hayat, G. Raviv, Reflection photo-plethysmography of arterial-blood-volume pulses, Med. Biol. Eng. Comput. 15 (1977) 22–31, https://doi.org/10.1007/BF02441571.
[22] V.C. Roberts, Photoplethysmography-fundamental aspects of the optical properties of blood in motion, Trans. Inst. Meas. Control 4 (1982) 101–106, https://doi.org/10.1177/014233128200400205.
[23] J.R. Jago, A. Murray, Repeatability of peripheral pulse measurements on ears, fingers and toes using photoelectric plethysmography, Clin. Phys. Physiol. Meas. 9 (1988) 319–329, https://doi.org/10.1088/0143-0815/9/4/003.
[24] S. Loukogeorgakis, R. Dawson, N. Philips, et al., Validation of a device to measure arterial pulse wave velocity by a photoplethysmographic method, Physiol. Meas. 23 (2002) 581–596, https://doi.org/10.1088/0967-3334/23/3/309.
[25] K.H. Shelley, D. Tamai, D. Jablonka, et al., The effect of venous pulsation on the forehead pulse oximeter wave form as a possible source of error in Spo2 calculation, Anesth. Analg. 100 (2005) 743–747, https://doi.org/10.1213/01.ANE.0000145063.01043.4B.
[26] B. Khanoka, Y. Slovik, D. Landau, M. Nitzan, Sympathetically induced spontaneous fluctuations of the photoplethysmographic signal, Med. Biol. Eng. Comput. 42 (2004) 80–85, https://doi.org/10.1007/BF02351014.
[27] J-M. Kim, K. Arakawa, K.T. Benson, D.K. Fox, Pulse oximetry and circulatory kinetics associated with pulse volume amplitude measured by photoelectric plethysmography, Anesth. Analg. 65 (1986) 1333–1339.
[28] W.B. Murray, P.A. Foster, The peripheral pulse wave: information overlooked, J. Clin. Monit. Comput. 12 (1996) 365–377, https://doi.org/10.1007/BF02077634.
[29] N. Selvaraj, A.K. Jaryal, J. Santhosh, et al., Assessment of heart rate variability derived from finger-tip photoplethysmography as compared to electrocardiography, J. Med. Eng. Technol. 32 (2008) 479–484, https://doi.org/10.1080/03091900701781317.
[30] G. Cenini, J. Arguel, K. Aksir, A. van Leest, Heart rate monitoring via remote photoplethysmography with motion artifacts reduction, Opt. Express 18 (2010) 4867–4875, https://doi.org/10.1364/OE.18.004867.
[31] A.A. Kamshilin, S. Miridonov, V. Teplov, et al., Photoplethysmographic imaging of high spatial resolution, Biomed. Opt. Express 2 (2011) 996–1006, https://doi.org/10.1364/BOE.2.000996.
[32] J. Allen, Photoplethysmography and its application in clinical physiological measurement, Physiol. Meas. 28 (2007) R1–R39, https://doi.org/10.1088/0967-3334/28/3/R01.
[33] A.A. Kamshilin, E. Nippolainen, I.S. Sidorov, et al., A new look at the essence of the imaging photoplethysmography, Sci. Rep. 5 (2015) 10494, https://doi.org/10.1038/srep10494.
[34] J.C. de Trefford, K. Lafferty, What does photo-plethysmography measure?, Med. Biol. Eng. Comput. 22 (1984) 479–480, https://doi.org/10.1007/BF02447713.
[35] C-Z. Wang, Y-P. Zheng, Comparison between reflection-mode photoplethysmography and arterial diameter change detected by ultrasound at the region of radial artery, Blood Press Monit. 15 (2010) 213–219, https://doi.org/10.1097/MBP.0b013e328338aada.
[36] P. Zaramella, F. Freato, V. Quaresima, et al., Foot pulse oximeter perfusion index correlates with calf muscle perfusion measured by near-infrared spectroscopy in healthy neonates, J. Perinatol. 25 (2005) 417–422, https://doi.org/10.1038/sj.jp.7211328.

[37] W. Verkruysse, L.O. Svaasand, J.S. Nelson, Remote plethysmographic imaging using ambient light, Opt. Express 16 (2008) 21434–21445, https://doi.org/10.1364/OE.16.021434.
[38] Y. Maeda, M. Sekine, T. Tamura, The advantages of wearable green reflected photoplethysmography, J. Med. Syst. 35 (2011) 829–850, https://doi.org/10.1007/s10916-010-9506-z.
[39] B.A. Fallow, T. Tarumi, H. Tanaka, Influence of skin type and wavelength on light wave reflectance, J. Clin. Monit. Comput. 27 (2013) 313–317, https://doi.org/10.1007/s10877-013-9436-7.
[40] R.R. Anderson, J.A. Parrish, Optical properties of human skin, in: J.D. Reganand, J.A. Parrish (Eds.), The Science of Photomedicine, Springer US, New York, 1982, pp. 147–194.
[41] A.N. Bashkatov, E.A. Genina, V.I. Kochubey, V.V. Tuchin, Optical properties of human skin, subcutaneous and mucous tissues in the wavelength range from 400 to 2000 nm, J. Phys. D, Appl. Phys. 38 (2005) 2543–2555, https://doi.org/10.1088/0022-3727/38/15/004.
[42] H. Gray, Anatomy of the Human Body, Churchill Livingstone Elsevier, Edinburgh, 2008.
[43] F. Mahler, M.H. Muheim, M. Intaglietta, et al., Blood pressure fluctuations in human nailfold capillaries, Am. J. Physiol. 236 (1979) H888–H893, https://doi.org/10.1152/ajpheart.1979.236.6.H888.
[44] S.A. Williams, S. Wasserman, D.W. Rawlinson, et al., Dynamic measurement of human capillary blood pressure, Clin. Sci. 74 (1988) 507–512, https://doi.org/10.1042/cs0740507.
[45] M.V. Volkov, N.B. Margaryants, A.V. Potemkin, et al., Video capillaroscopy clarifies mechanism of the photoplethysmographic waveform appearance, Sci. Rep. 7 (2017) 13298, https://doi.org/10.1038/s41598-017-13552-4.
[46] Y.C. Fung, B.W. Zweifach, M. Intaglietta, Elastic environment of the capillary bed, Circ. Res. 19 (1966) 441–461, https://doi.org/10.1161/01.RES.19.2.441.
[47] L.S. D'Agrosa, A.B. Hertzman, Opacity pulse of individual minute arteries, J. Appl. Physiol. 23 (1967) 613–620, https://doi.org/10.1152/jappl.1967.23.5.613.
[48] G.H. Weiss, R. Nossal, R.F. Bonner, Statistics of penetration depth of photons re-emitted from irradiated tissue, J. Mod. Opt. 36 (1989) 349–354, https://doi.org/10.1080/09500348914550381.
[49] S. Chatterjee, K. Budidha, P.A. Kyriacou, Investigating the origin of photoplethysmography using a multiwavelength Monte Carlo model, Physiol. Meas. (2020), https://doi.org/10.1088/1361-6579/aba008.
[50] W. Verkruysse, M. Bartula, E. Bresch, et al., Calibration of contactless pulse oximetry, Anesth. Analg. 124 (2017) 136–145, https://doi.org/10.1016/10.1213/ANE.0000000000001381.
[51] F. Corral, G. Paez, M. Strojnik, A photoplethysmographic imaging system with supplementary capabilities, Opt. Appl. 44 (2014) 191–204, https://doi.org/10.5277/oa140202.
[52] K. Humphreys, T. Ward, C. Markham, Noncontact simultaneous dual wavelength photoplethysmography: a further step toward noncontact pulse oximetry, J. Opt. Soc. Am. Rev. Sci. Instrum. 78 (2007) 44304, https://doi.org/10.1063/1.2724789.
[53] E.K. Chan, B. Sorg, D. Protsenko, et al., Effects of compression on soft tissue optical properties, IEEE J. Sel. Top. Quantum Electron. 2 (1996) 943–950, https://doi.org/10.1109/2944.577320.
[54] E. Nippolainen, N.P. Podolian, R.V. Romashko, et al., Photoplethysmographic waveform as a function of subject's age, Phys. Proc. 73 (2015) 241–245, https://doi.org/10.1016/j.phpro.2015.09.164.
[55] A.A. Kamshilin, O.V. Mamontov, V.T. Koval, et al., Influence of a skin status on the light interaction with dermis, Biomed. Opt. Express 6 (2015) 4326–4334, https://doi.org/10.1364/BOE.6.004326.
[56] I.S. Sidorov, R.V. Romashko, V.T. Koval, et al., Origin of infrared light modulation in reflectance-mode photoplethysmography, PLoS ONE 11 (2016) e0165413, https://doi.org/10.1371/journal.pone.0165413.
[57] A.C.M. Dassel, R. Graaff, A. Meijer, et al., Reflectance pulse oximetry at the forehead of newborns. The influence of varying pressure on the probe, J. Clin. Monit. Comput. 12 (1996) 421–428, https://doi.org/10.1007/BF02199702.

[58] X-F. Teng, Y-T. Zhang, The effect of contacting force on photoplethysmographic signals, Physiol. Meas. 25 (2004) 1323–1335, https://doi.org/10.1088/0967-3334/25/5/020.
[59] A.R. Guazzi, M.C. Villarroel, J. Jorge, et al., Non-contact measurement of oxygen saturation with an RGB camera, Biomed. Opt. Express 6 (2015) 3321–3338, https://doi.org/10.1364/BOE.6.003320.
[60] R.F. Schmidt, G. Thews, Human Physiology, Springer-Verlag, Berlin, Heidelberg, 1989.
[61] P.B. Canham, A.C. Burton, Distribution of size and shape in populations of normal human red cells, Circ. Res. 22 (1968) 405–422, https://doi.org/10.1161/01.RES.22.3.405.
[62] L-G. Lindberg, P.Å Öberg, Optical properties of blood in motion, Opt. Eng. 32 (1993) 253–257, https://doi.org/10.1117/12.60688.
[63] A.M.K. Enejder, J. Swartling, P. Aruna, S. Andersson-Engels, Influence of cell shape and aggregate formation on the optical properties of flowing whole blood, Appl. Opt. 42 (2003) 1384–1394, https://doi.org/10.1364/AO.42.001384.
[64] N.B. Margaryants, I.S. Sidorov, M.V. Volkov, et al., Visualization of skin capillaries with moving red blood cells in arbitrary area of the body, Biomed. Opt. Express 10 (2019) 4896–4906, https://doi.org/10.1364/BOE.10.004896.
[65] S. Shin, Y. Yang, J-S. Suh, Measurement of erythrocyte aggregation in a microchip stirring system by light transmission, Clin. Hemorheol. Microcirc. 41 (2009) 197–207, https://doi.org/10.3233/CH-2009-1172.
[66] I.B. Wilkinson, D.J. Webb, Venous occlusion plethysmography in cardiovascular research: methodology and clinical applications, Br. J. Clin. Pharmacol. 52 (2001) 631–646, https://doi.org/10.1046/j.1365-2125.2001.01495.x.
[67] R.A. Bays, D.A. Healy, R.G. Atnip, et al., Validation of air plethysmography, photoplethysmography, and duplex ultrasonography in the evaluation of severe venous stasis, J. Vasc. Surg. 20 (1994) 721–727, https://doi.org/10.1016/S0741-5214(94)70159-8.
[68] A.A. Kamshilin, V.V. Zaytsev, O.V. Mamontov, Novel contactless approach for assessment of venous occlusion plethysmography by video recordings at the green illumination, Sci. Rep. 7 (2017) 464, https://doi.org/10.1038/s41598-017-00552-7.
[69] V.V. Zaytsev, S.V. Miridonov, O.V. Mamontov, A.A. Kamshilin, Contactless monitoring of the blood-flow changes in upper limbs, Biomed. Opt. Express 9 (2018) 5387–5399, https://doi.org/10.1364/BOE.9.005387.
[70] C.E. Dunn, B. Lertsakdadet, C. Crouzet, et al., Comparison of speckleplethysmographic (SPG) and photoplethysmographic (PPG) imaging by Monte Carlo simulations and in vivo measurements, Biomed. Opt. Express 9 (2018) 4306–4316, https://doi.org/10.1364/BOE.9.004306.
[71] V.V. Zaytsev, O.V. Mamontov, A.A. Kamshilin, Assessment of cutaneous blood flow in lower extremities by imaging photoplethysmography method, Sci. Tech. J. Inf. Technol. Mech. Opt. 19 (2019) 994–1004, https://doi.org/10.17586/2226-1494-2019-19-6-994-1003.
[72] H. Nonaka, M. Akima, T. Nagayama, et al., Microvasculature of the human cerebral meninges, Neuropathology 23 (2003) 129–135, https://doi.org/10.1046/j.1440-1789.2003.00487.x.
[73] O.A. Lyubashina, O.V. Mamontov, M.A. Volynsky, et al., Contactless assessment of cerebral autoregulation by photoplethysmographic imaging at green illumination, Front. Neurosci. 13 (2019) 1235, https://doi.org/10.3389/fnins.2019.01235.
[74] O.V. Mamontov, A.V. Shcherbinin, R.V. Romashko, A.A. Kamshilin, Intraoperative imaging of cortical blood flow by camera-based photoplethysmography at green light, Appl. Sci. 10:6192 (2020), https://doi.org/10.3390/app10186192.
[75] O.B. Paulson, S. Strandgaard, L. Edvinsson, Cerebral autoregulation, Cerebrovasc. Brain Metab. Rev. 2 (1990) 161–192.
[76] C.K. Willie, Y-C. Tzeng, J.A. Fisher, P.N. Ainslie, Integrative regulation of human brain blood flow, J. Physiol. 592 (2014) 841–859, https://doi.org/10.1113/jphysiol.2013.268953.
[77] S. Fantini, A. Sassaroli, K.T. Tgavalekos, J. Kornbluth, Cerebral blood flow and autoregulation: current measurement techniques and prospects for noninvasive optical methods, Neurophotonics 3 (2016) 31411, https://doi.org/10.1117/1.NPh.3.3.031411.

[78] E. Hamel, Perivascular nerves and the regulation of cerebrovascular tone, J. Appl. Physiol. 100 (2006) 1059, https://doi.org/10.1152/japplphysiol.00954.2005.

[79] H. Holst, L. Arendt-Nielsen, H. Mosbech, et al., Capsaicin-induced neurogenic inflammation in the skin in patients with symptoms induced by odorous chemicals, Skin Res. Technol. 17 (2011) 82–90, https://doi.org/10.1111/j.1600-0846.2010.00470.x.

[80] F.A. Russell, R. King, S.J. Smillie, et al., Calcitonin gene-related peptide: physiology and pathophysiology, Physiol. Rev. 94 (2014) 1099–1142, https://doi.org/10.1152/physrev.00034.2013.

[81] B. Fromy, A. Josset-Lamaugarny, G. Aimond, et al., Disruption of TRPV3 impairs heat-evoked vasodilation and thermoregulation: a critical role of CGRP, J. Invest. Dermatol. 138 (2018) 688–696, https://doi.org/10.1016/j.jid.2017.10.006.

[82] A.A. Kamshilin, A.V. Belaventseva, R.V. Romashko, et al., Local thermal impact on microcirculation assessed by imaging photoplethysmography, Biol. Med. 8 (2016) 1000361, https://doi.org/10.4172/0974-8369.1000361.